

Effect of hydroxyl group position on adsorption behavior and corrosion inhibition of hydroxybenzaldehyde Schiff bases: Electrochemical and quantum calculations

I. Danaee^{a,*}, O. Ghasemi^a, G.R. Rashed^a, M. Rashvand Avei^b, M.H. Maddahy^a

^aAbadan Faculty of Petroleum Engineering, Petroleum University of Technology, Abadan, Iran

^bDepartment of Chemistry, K.N. Toosi University of Technology, Tehran, Iran

HIGHLIGHTS

- ▶ The inhibition ability of Schiff bases against the corrosion of steel was evaluated.
- ▶ Schiff bases retard both the cathodic and anodic reactions through chemical adsorption.
- ▶ The correlation of inhibition effect and molecular structure was discussed.
- ▶ Frontier orbital theory which was applied to the results of quantum chemistry.

ARTICLE INFO

Article history:

Received 16 May 2012

Received in revised form 5 November 2012

Accepted 7 November 2012

Available online 16 November 2012

Keywords:

Inhibition

Schiff base

AFM

Density functional theory (DFT)

Ab initio calculation

ABSTRACT

The corrosion inhibition and adsorption of *N,N'*-bis(*n*-hydroxybenzaldehyde)-1,3-propandiimine (*n*-HBP) Schiff bases has been investigated on steel electrode in 1 M HCl by using electrochemical techniques. The experimental results suggest that the highest inhibition efficiency was obtained for 3-HBP. Polarization curves reveal that all studied inhibitors are mixed type. Density functional theory (DFT) at the B3LYP/6-31G(d,p) and B3LYP/3-21G basis set levels and ab initio calculations using HF/6-31G(d,p) and HF/3-21G methods were performed on three Schiff bases. By studying the effects of hydroxyl groups in ortho-, meta-, para- positions, the best one as inhibitor was found to be meta-position of OH in Schiff base (i.e., 3-HBP). The order of inhibition efficiency obtained was corresponded with the order of most of the calculated quantum chemical parameters. Quantitative structure activity relationship (QSAR) approach has been used and a correlation of the composite index of some of the quantum chemical parameters was performed to characterize the inhibition performance of the Schiff bases studied. The results showed that %IE of the Schiff bases was closely related to some of the quantum chemical parameters but with varying degrees/order. The calculated %IE of the Schiff base studied was found to be close to their experimental corrosion inhibition efficiencies.

© 2012 Elsevier B.V. All rights reserved.

1. Introduction

Acid solutions with pH values below one are generally used for industrial acid cleaning, acid descaling, oil well acidizing, the pickling and removal of undesirable rust [1–3]. Mild steel which are extensively used in a lot of industrial processes, could corrode during these acidic applications particularly with the use of HCl [4,5].

Corrosion prevention systems favor the use of corrosion inhibitors with low or zero environmental impacts. Inhibitors are chemicals that react with a metallic surface or the environment. Inhibitors decrease corrosion processes by, increasing the anodic or cathodic polarization behavior, reducing the movement or

diffusion of ions to the metallic surface and increasing the electrical resistance of the metallic surface [6].

The use of organic molecules as corrosion inhibitor is one of the most practical methods for protecting against the corrosion and it is becoming increasingly popular. These compounds in general are adsorbed on the metal surface, blocking the active corrosion sites. Four types of adsorption may take place by organic molecules at metal/solution interface:

- (a) electrostatic attraction between the charged molecules and the charged metal
- (b) interaction of unshared electron pairs in the molecule with the metal
- (c) interaction of π -electrons with the metal
- (d) combination of a and c

* Corresponding author. Tel.: +98 631 4429937.

E-mail address: danaee@put.ac.ir (I. Danaee).

Nomenclature

β_a, β_c	anodic and cathodic Tafel slopes	I_{corr}	corrosion current
μ	dipole moment, electronic chemical potential	IE	inhibition efficiency
2-HBP	N,N'-bis(2-hydroxybenzaldehyde)-1,3-propanediimine	IE_{exp}	Experimental inhibition efficiency
3-HBP	N,N'-bis(3-hydroxybenzaldehyde)-1,3-propanediimine	IE_{Theor}	Theoretical inhibition efficiency
4-HBP	N,N'-bis(4-hydroxybenzaldehyde)-1,3-propanediimine	LUMO	lowest unoccupied molecular orbital
A	electron affinity	MO	molecular orbital
AFM	atomic Force Microscopy	NLM	nonlinear model
C	capacitor	n	Q_{dl} exponent
C_{dl}	double layer capacitance	Q_{dl}	double layer constant phase element
CPE	constant Phase Element (Q)	QSAR	quantitative structure activity relationship
DFT	density functional theory	R_{ct}	charge transfer resistance
E_{corr}	corrosion potential	R_p	polarization resistance
EIS	electrochemical impedance spectroscopy	SCE	saturated Calomel Electrode
f	frequency	ΔE	energy gap
HF	Hartree–Fock	ΔN	fraction of charge transferred
HOMO	highest occupied molecular orbital	η	absolute hardness
I	ionization potential	χ	absolute electronegativity

The adsorption ability of inhibitors onto metal surface depends on the nature and surface charge of metal, the chemical composition of electrolytes, and the molecular structure and electronic characteristics of inhibitor molecules. It was shown that organic compounds containing heteroatoms such as nitrogen, sulfur, oxygen and phosphorus are capable of forming coordinate covalent bond with metal owing to their free electron pairs and thus acting as inhibitor. The conjugated double bonds or π electrons in triple bonds exhibit good inhibitive properties [7–9]. Schiff bases (with RC = NR' as general formula) have the both features combined with their structure which may then give rise to particularly potential inhibitors [10]. Schiff bases are condensation products of an amine and a ketone or aldehyde and the first Schiff base metal complexes were prepared and described in the literature by Schiff in (1864). An interesting phenomenon is that Schiff bases systematically display considerably stronger corrosion inhibition efficiencies than the corresponding amines. Schiff bases have been recently reported as effective corrosion inhibitors for steel, aluminum and copper in acidic media. The greatest advantages of Schiff bases are [11,12]:

- they can be synthesized conveniently from inexpensive raw materials
- they contain the electron cloud on the aromatic ring or, the electronegative atoms such as nitrogen and oxygen in the relatively long chain compounds
- harmless for environment

Theoretical chemistry has been used recently to explain the mechanism of corrosion inhibition, such as quantum chemical calculations [13,14]. Quantum chemical calculations have been proven to be a very powerful tool for studying the mechanism [15,16]. The objective of this work is to present the relationships between the Schiff bases reactivity and their ability to inhibit the corrosion of mild steel in hydrochloric acid to understand if any structural differences induced by different positions of the hydroxyl group may be related to the experimentally observed differences of corrosion efficiency. The structural parameters, such as the frontier molecular orbital energy HOMO (highest occupied molecular orbital) and LUMO (lowest unoccupied molecular orbital), the charge distribution of the studied inhibitors, the absolute electronegativity (χ) values, and the fraction of electrons (ΔN) transfer from inhibitors to iron were calculated and correlated with inhibition efficiencies.

2. Experimental and computational details

2.1. Material preparation

All chemicals used in present work were of reagent-grade Merck product and used as received without further purification. The three Schiff bases were prepared according to the described procedure [17]. The compounds were synthesized from 1:2 mol ratios of 1,3-diaminopropane and *n*-Hydroxybenzaldehyde (2-, 3- and 4-hydroxybenzaldehyde) through a condensation reaction in ethanolic media then recrystallized in ethanol. The physical and analytical data for the Schiff bases is given in Table 1. Identification of structure of synthesized Schiff base was performed by IR, ^1H NMR and ^{13}C -NMR spectroscopic techniques. The Schiff base derivatives used in this study are presented in Fig. 1.

2.2. Computational techniques

All the quantum chemical calculations were performed with complete geometry optimizations using standard Gaussian-03 software package [18]. Geometry optimization were carried out by two different methods: ab initio methods at the Hartree–Fock (HF) level with the 3-21G and 6-31G(d,p) basis sets and at the density functional theory (DFT) level with the non-local hybrid density functional B3LYP [19], combining Becke's three-parameter hybrid exchange functional with the correlation functional of Lee et al. [20] at basis sets 3-21G and 6-31G(d,p) [21,22].

Statistical analyses were performed using SPSS program version 15.0 for windows. Non-linear regression analyses were performed by unconstrained sum of squared residuals for loss function and estimation methods of Levenberg–Marquardt using SPSS program version 15.0 for windows.

2.3. Electrochemical measurements

Working electrodes were prepared from steel specimens of the chemical composition (wt.%) C = 0.16%, Si = 0.32%, Mn = 0.35%, P = 0.03%, S = 0.02%, and the remainder Fe. Samples were cut from a cylindrical rod with a cutter machine. The exposed surface area of each electrode is equal to 0.81 cm². These specimens were used as working electrode in electrochemical measurements and the exposed areas of the electrodes were mechanically abraded with 220, 400, 600, 800, 1000 and 1200 grades of emery paper,

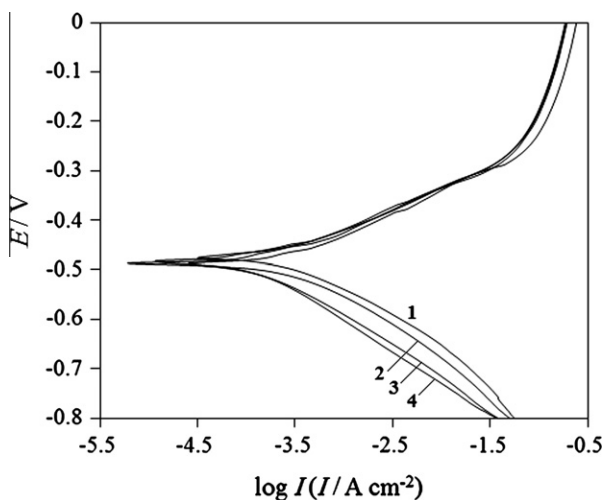


Fig. 2. Tafel polarization curves for steel in 1 M HCl (1), in the presence of 5×10^{-5} M of 2-HBP (2), 4-HBP (3) and 3-HBP (4).

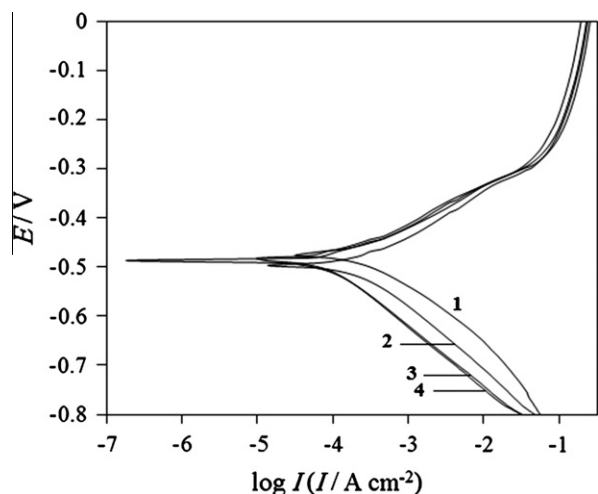


Fig. 3. Tafel polarization curves for steel in 1 M HCl (1), in the presence of 2×10^{-4} M of 2-HBP (2), 4-HBP (3) and 3-HBP (4).

for different concentrations of inhibitor is calculated using the following equations [7,25]:

$$\theta = \left(\frac{i_{\text{corr}} - i_{\text{corr}}}{i_{\text{corr}}} \right) \quad (1)$$

$$IE\% = \left(\frac{i_{\text{corr}} - i_{\text{corr}}}{i_{\text{corr}}} \right) \times 100 \quad (2)$$

where i_{corr} and I_{corr} are the corrosion current densities determined by the intersection of the extrapolated Tafel lines and the corrosion potential for steel in uninhibited and inhibited acid solution, respectively.

As was expected both anodic and cathodic reactions of steel electrode corrosion were inhibited with the increase of the inhibitors concentration. This result suggests that the addition of the inhibitors reduces anodic dissolution and also retards the hydrogen evolution reaction [26]. The electrochemical processes on the metal surface are related to the adsorption of the inhibitors and the adsorption is known to depend on the chemical structure of the inhibitors. The parallel cathodic Tafel curves in Figs. 2 and 3

show that the hydrogen evolution is activation-controlled and the reduction mechanism is not affected by the presence of the inhibitors. No definite trend was observed in the shift of E_{corr} values in the presence of different concentrations of the inhibitors, suggesting that these compounds behave as mixed-type inhibitors [27]. However, the influence is more pronounced in the cathodic polarization plots compared to that in the anodic polarization plots. It is clear that the addition of the inhibitor shifts the cathodic curves to a greater extent toward the lower current density when compared to the anodic curves. The E_{corr} value is also shifted to the more negative side with an increase in the inhibitor concentration [28]. It can be seen that the corrosion rate decreased and inhibition efficiency ($IE\%$) increased by increasing inhibitor concentration. Polarization resistance (R_p) values were determined from the slope of the polarization curve and calculated using Stern–Geary equation which is given below [29,30]:

$$R_p = \frac{\beta_a \cdot \beta_c}{2.303(\beta_a + \beta_c)} \times \frac{1}{i_{\text{corr}}} \quad (3)$$

By increasing the inhibitors concentration the polarization resistance increases in the presence of compound, indicating adsorption of the inhibitor on the metal surface to block the active sites efficiently and inhibit corrosion [31].

3.2. Electrochemical impedance spectroscopy

Figs. 4 and 5 show Nyquist plots for steel in 1 M HCl solution in the presence of 5×10^{-5} and 2×10^{-4} M of 2-, 3- and 4-HBP. The plots show a depressed capacitive loop which arises from the time constant of the electrical double layer and charge transfer resistance. As can be seen, higher charge transfer resistance was obtained in presence of 3-HBP. The impedance of the inhibited steel increases with increasing the inhibitor's concentration and consequently the inhibition efficiency increases. The equivalent circuit compatible with the Nyquist diagram recorded in the presence of inhibitors was depicted in Fig. 6.

The simplest approach requires the theoretical transfer function $Z(\omega)$ to be represented by a parallel combination of a resistance R_{ct} and a capacitance C , both in series with another resistance R_s [32]:

$$Z(\omega) = R_s + \frac{1}{1/R_{ct} + i\omega C} \quad (4)$$

ω is the frequency in rad/s, $\omega = 2\pi f$ and f is frequency in Hz.

To obtain a satisfactory impedance simulation of steel, it is necessary to replace the capacitor (C) with a constant phase element (CPE) Q in the equivalent circuit. The most widely accepted explanation for the presence of CPE behavior and depressed semicircles on solid electrodes is microscopic roughness, causing an inhomogeneous distribution in the solution resistance as well as in the double-layer capacitance [33]. Constant phase element CPE_{dl} , R_s and R_{ct} can be corresponded to double layer capacitance, solution resistance, and charge transfer resistance respectively. To corroborate the equivalent circuit, the experimental data are fitted to equivalent circuit and the circuit elements are obtained. Table 3 illustrates the equivalent circuit parameters for the impedance spectra of corrosion of steel in 1 M HCl solution. The results demonstrate that the presence of inhibitors enhance the value of R_{ct} obtained in the pure medium while that of Q_{dl} is reduced. The decrease in Q_{dl} values was caused by adsorption of inhibitor indicating that the exposed area decreased. On the other hand, a decrease in Q_{dl} , which can result from a decrease in local dielectric constant and/or an increase in the thickness of the electrical double layer, suggests that Schiff base inhibitors act by adsorption at the metal–solution interface.

Table 2
Potentiodynamic polarization parameters for the corrosion of mild steel in 1 M HCl solution in absence and presence of different concentrations of *n*-HBP.

Inhibitor	Concen. (M)	$-E_{corr}$ (mV)	I_{corr} ($\mu\text{A cm}^{-2}$)	Corrosion rate (mpy)	β_a (mV dec^{-1})	$-\beta_c$ (mV dec^{-1})	R_p ($\Omega \text{ cm}^2$)	θ	IE%
2-HBP	Blank	442	710	324.5	84	111	29	–	–
	5×10^{-5}	485	294	134.3	80	146	76	0.58	58
	2×10^{-4}	495	270	123.4	95.7	133	90	0.62	62
3-HBP	5×10^{-5}	496	173	79.1	91.2	126	133	0.76	76
	2×10^{-4}	499	114	52.1	83	124	189	0.84	84
4-HBP	5×10^{-5}	481	242	110.6	87.5	138	96	0.66	66
	2×10^{-4}	499	128	58.5	87.3	123	173	0.82	82

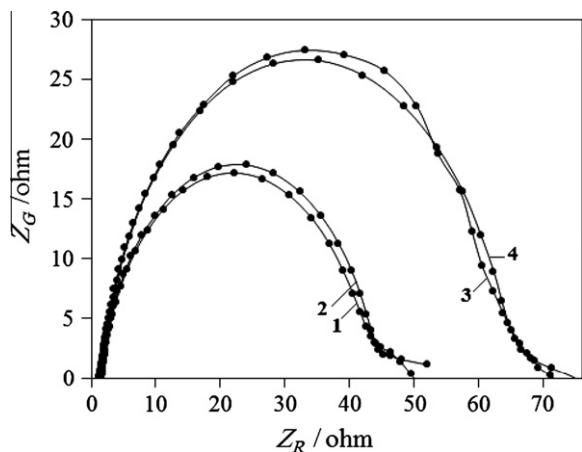


Fig. 4. Nyquist plots for steel in 1 M HCl (1) in the presence of 5×10^{-5} M of 2-HBP (2), 4-HBP (3) and 3-HBP (4).

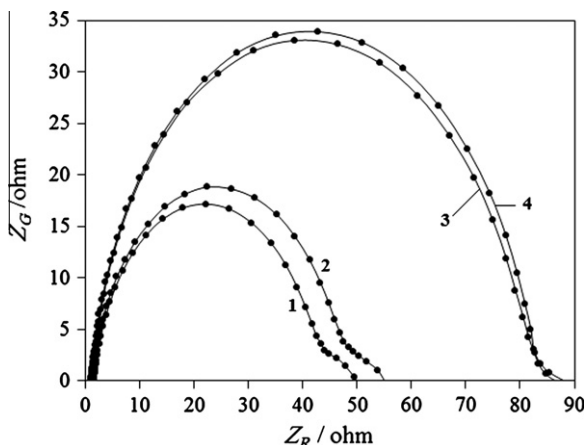


Fig. 5. Nyquist plots for steel in 1 M HCl (1) in the presence of 2×10^{-4} M of 2-HBP (2), 4-HBP (3) and 3-HBP (4).

As the Q_{dl} exponent (n) is a measure of the surface heterogeneity, values of n indicates that the steel surface becomes more and more homogeneous as the concentration of inhibitor increases as a result of its adsorption on the steel surface and corrosion inhibition. The increase in values of R_{ct} and the decrease in values of Q_{dl} with increasing the concentration also indicate that Schiff bases act as primary interface inhibitors and the charge transfer controls the corrosion of steel under the open circuit conditions.

3.3. Chronoamperometry

In order to gain more insight about the effect of inhibitors on the electrochemical behavior of steel in 1 M HCl solution,

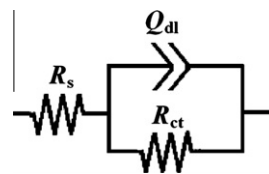


Fig. 6. Equivalent circuits compatible with the experimental impedance data in Figs. 4 and 5.

Table 3
Impedance data for mild steel in 1 M HCl solution without and with different concentrations of *n*-HBP.

Inhibitor	Concen (M)	R_s (Ω)	R_{ct} (Ω)	$Q_{dl} \times 10^3$ (F)	n
2-HBP	Blank	1.5	42	2.5	0.86
	5×10^{-5}	1.5	44	1.8	0.88
	2×10^{-4}	1.4	47	1.5	0.88
3-HBP	5×10^{-5}	1.5	65	0.7	0.9
	2×10^{-4}	1.4	81	0.5	0.92
4-HBP	5×10^{-5}	1.5	63	1.3	0.9
	2×10^{-4}	1.4	81	0.7	0.89

potentiostatic current–time transients were recorded. Fig. 7 shows the current transients of steel electrode at -0.4 V vs. SCE applied anodic potential. Initially the current decreases monotonically with time. The decrease in the current density is due to the formation of corrosion products layer on the anode surface. However, in later times the current increases tracing approximately a straight line to reach a steady state value depending on applied potential (Fig. 7). The increase in current is related to the dissolution of the steel and pit nucleation and pit growth. In presence of inhibitor, increasing current was not observed and electrode was inhibited from corrosion due to inhibitor adsorption.

3.4. Molecular structure and quantum chemical calculation

The effectiveness of an inhibitor is related to its spatial molecular structure as well as with its molecular electronic structure [34]. In this regard, quantum chemical calculations have proved to be a powerful tool for studying corrosion inhibition mechanism and recently, corrosion publications have contained substantial quantum chemical calculations [35,36]. In this study, quantum chemical calculations were conducted at two different methods: ab initio methods at the Hartree–Fock (HF) level and the density functional theory (DFT) level with the 3-21G and 6-31G(d,p) basis sets by geometry optimization of the studied compounds in order to support experimental data and to investigate the relationship between molecular structure of the Schiff bases and their inhibition effects.

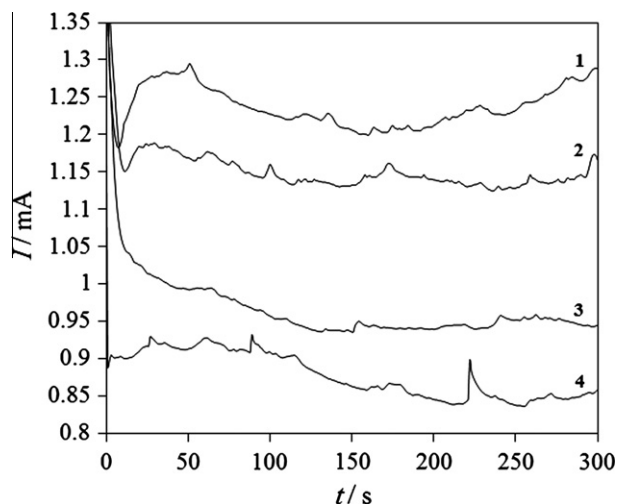


Fig. 7. Current transients of steel electrode at -0.4 V vs. SCE: (1) Blank, (2) 2×10^{-4} M of 2-HBP, (3) 4-HBP and (4) 3-HBP.

Table 4

Selected bond lengths (in angstroms) and bond angles (in degrees) of the *n*-HBP Schiff bases with B3LYP/6-31G(d,p).

	2-HBP	3-HBP	4-HBP
<i>Bond lengths</i>			
C ₁ –N ₂	1.29	1.29	1.29
N ₂ –C ₃	1.47	1.47	1.47
C ₃ –C ₄	1.54	1.54	1.54
C ₄ –C ₅	1.54	1.54	1.54
C ₅ –N ₆	1.47	1.47	1.47
N ₆ –C ₇	1.28	1.29	1.29
(C–C) _{Ar}	1.40	1.40	1.40
C–O	1.39	1.39	1.39
<i>Bond angles</i>			
C ₁ –N ₂ –C ₃	119.14	124.43	119.44
N ₂ –C ₃ –C ₄	110.51	110.22	110.41
C ₃ –C ₄ –C ₅	112.09	114.24	111.51
C ₄ –C ₅ –N ₆	109.34	109.76	118.74
C ₅ –N ₆ –C ₇	123.16	124.71	122.24
C ₁ –N ₂ –C ₃ –C ₄	120.46	–144.95	121.65
N ₂ –C ₃ –C ₄ –C ₅	174.26	–61.56	174.44
C ₄ –C ₅ –N ₆ –C ₇	143.57	133.44	0.15
C ₃ –C ₄ –C ₅ –N ₆	175.66	–63.44	179.53

Fig. 8 represents the optimized structure of three Schiff bases. The selected bond lengths and bond angles for the studied Schiff bases are presented in Table 4. It could be easily seen that, molecules are not fully planar, which may result in relatively weak interaction between molecules and metal surface. However, different factors need to be considered for elucidating the orientation of organic molecules on the electrode surface. The atoms and groups of the molecules may interact with the electrode surface depend on the geometry of the inhibitor as well as the nature of their frontier molecular orbitals. Frontier molecular orbital (HOMO and LUMO) theory is useful in predicting the adsorption centers of the inhibitor responsible for the interaction with metal surface [35,37]. The HOMO and LUMO populations of the studied Schiff

bases are shown in Fig. 9. It can be seen in Fig. 9 that, the frontier molecular orbital distribution obtained from four different calculation methods have given very close results. Three Schiff bases investigated in the present study consist of symmetrical two parts and contain two benzene rings and two imine groups. Difference between the structures is related with the position of the substitution of OH group at ortho, meta and para position. It can be seen in Fig. 9 that, the HOMO location of 2-HBP Schiff base is relatively distributed throughout the molecule while the HOMO location of 3-HBP and 4-HBP Schiff bases are distributed over the benzene ring and a small part of the carbon chain that take place one side of the molecule. According to HOMO distribution of Schiff bases, it can be said that 3-HBP and 4-HBP molecules carry their rich

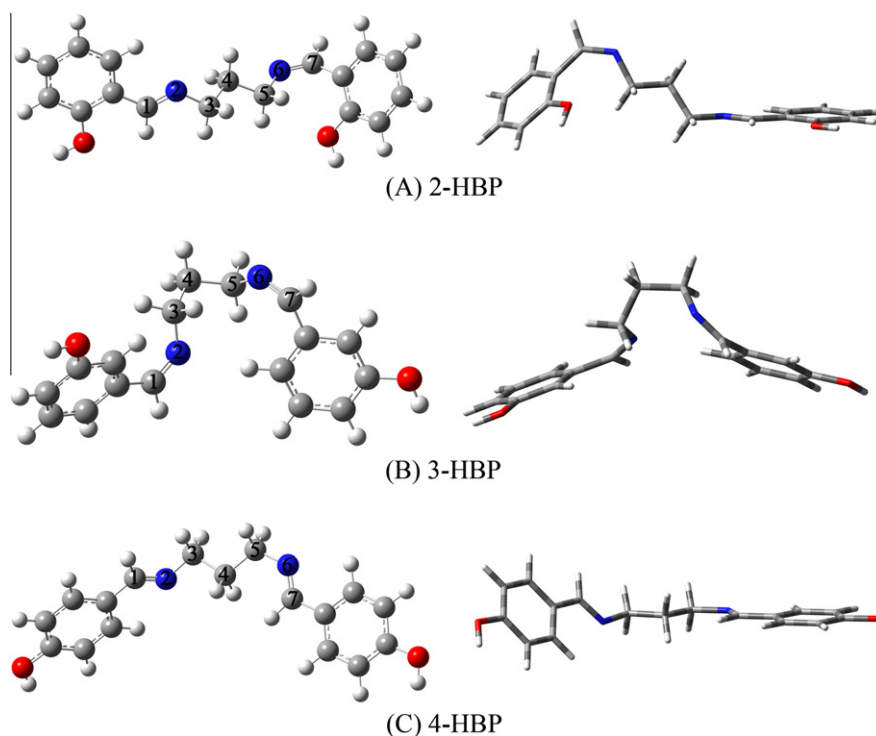


Fig. 8. The optimized structure of three *n*-HBP Schiff bases obtained at the B3LYP level (right) 'side on' view of the optimized structure.

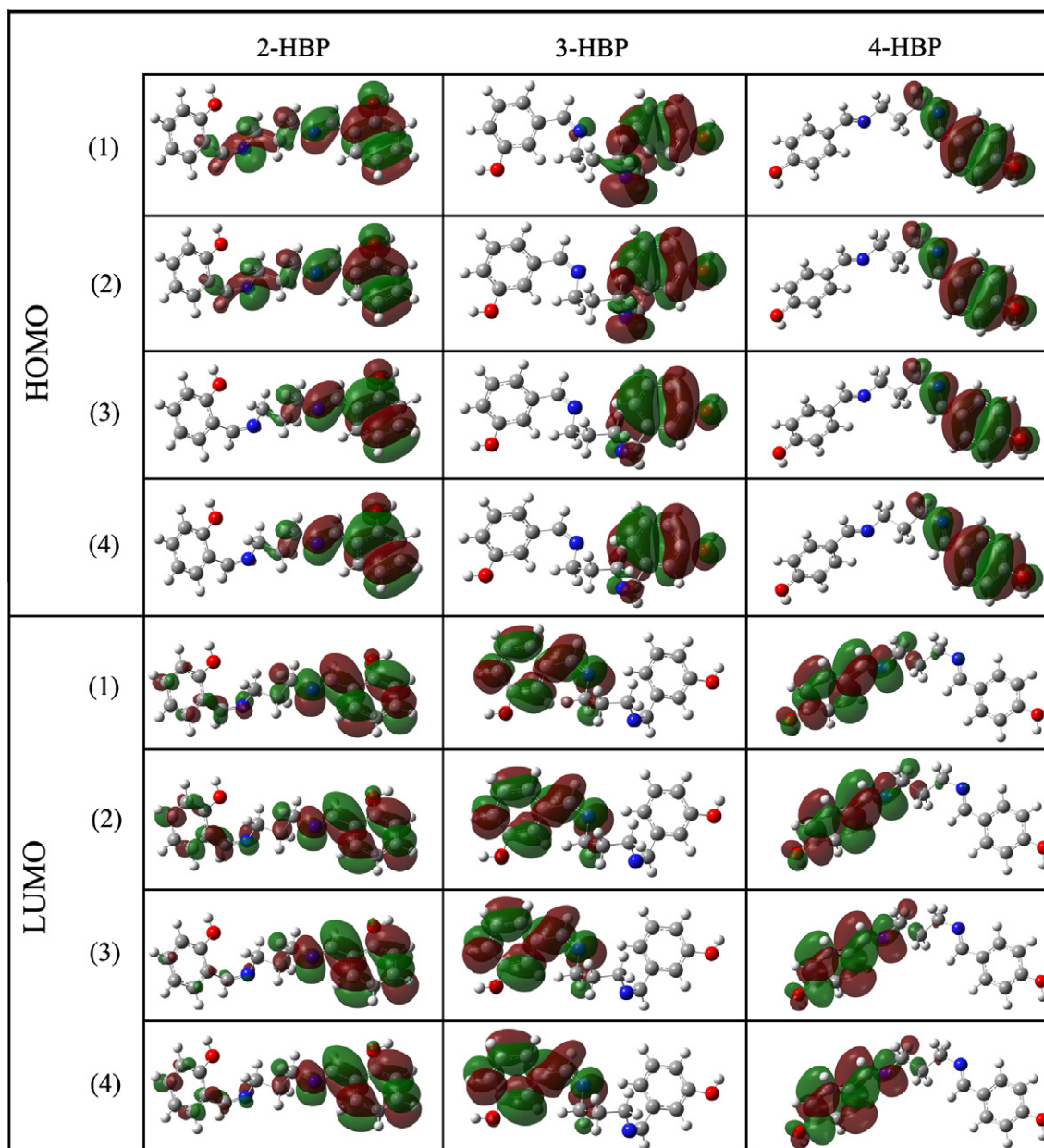


Fig. 9. HOMO and LUMO populations of investigated Schiff bases obtained at (1) B3LYP/6-31G(d,p), (2) B3LYP/3-21G, (3) RHF/6-31G(d,p) and (4) RHF/3-21G.

Table 5
Quantum chemical parameters for the studied Schiff bases.

Inhibitor	Models	E_{LUMO} (eV)	E_{HOMO} (eV)	$E_{\text{LUMO}}-E_{\text{HOMO}}$ (eV)	ΔN	μ (Debye)	Molar volume ($\text{cm}^3 \text{mol}^{-1}$)	%IE
2-HBP	DFT-B3LYP (6-31G(d,p))	-0.98	-5.97	4.99	0.7063	3.31	207.051	57
	DFT-B3LYP (3-21G)	-0.81	-5.87	5.06	0.7236	3.52	255.653	
	HF (6-31G(d,p))	2.90	-8.40	11.29	0.3763	3.22	194.940	
	HF (3-21G)	3.08	-8.39	11.47	0.3787	3.23	246.565	
4-HBP	DFT-B3LYP (6-31G(d,p))	-1.07	-5.91	4.84	0.7252	3.12	216.316	73
	DFT-B3LYP (3-21G)	-0.87	-5.80	4.93	0.7435	3.08	179.647	
	HF (6-31G(d,p))	2.83	-8.28	11.11	0.3852	2.87	195.121	
	HF (3-21G)	3.04	-8.27	11.31	0.3877	2.70	204.090	
3-HBP	DFT-B3LYP (6-31G(d,p))	-1.28	-5.95	4.67	0.7253	5.41	214.001	81
	DFT-B3LYP (3-21G)	-1.07	-5.81	4.75	0.7497	4.83	204.778	
	HF (6-31G(d,p))	2.72	-8.54	11.26	0.3634	5.62	190.780	
	HF (3-21G)	2.97	-8.49	11.46	0.3704	5.20	189.178	

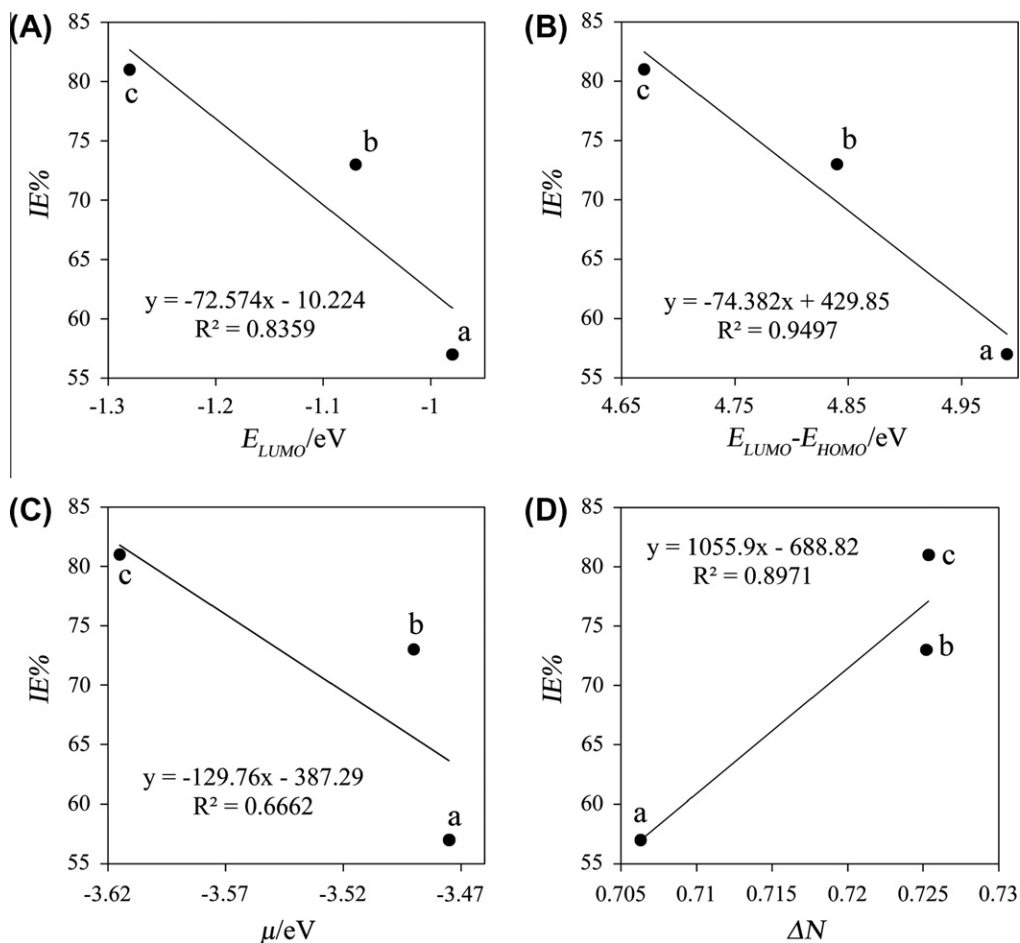


Fig. 10. Variation of experimental inhibition efficiency (IE%) with (A) the LUMO energy, (B) the HOMO–LUMO gap, (C) the electronic chemical potential and (D) ΔN of *n*-HBP Schiff bases: (a) 2-HBP, (b) 4-HBP and (c) 3-HBP.

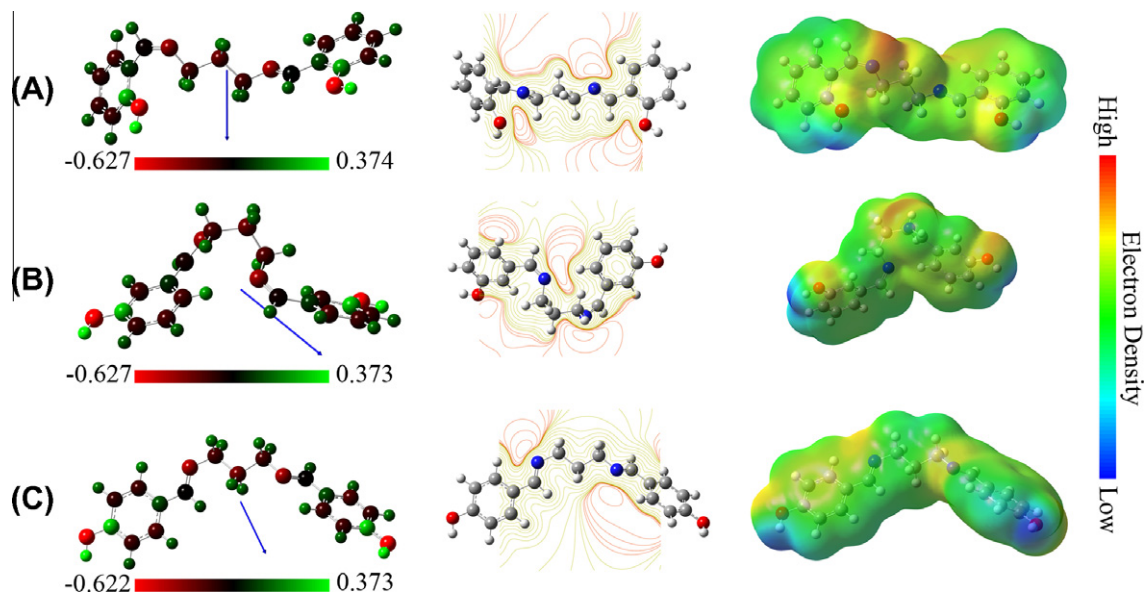


Fig. 11. Electrostatic properties of (A) 2-HBP (B) 3-HBP and (C) 4-HBP: side views of the dipole and the Mulliken charge populations are displayed on the left while the middle and right panels show the contour and isosurface representation of electrostatic potential respectively (the electron rich region is red and the electron poor region is blue). (For interpretation of the references to color in this figure legend, the reader is referred to the web version of this article.)

negative centers in a small region, in comparison with 2-HBP molecule. The parts of the molecules with low HOMO density probably more oriented towards to cathodic sites of the steel surface and afterwards adsorption occurs by sharing of electrons. Computed E_{HOMO} , E_{LUMO} , $E_{\text{LUMO}} - E_{\text{HOMO}}$, ΔN and molar volume values of studied Schiff bases were listed in Table 5. In order to investigate the agreement of the quantum chemical results with experimental observation, the measured inhibition efficiencies (%) of these three *n*-HBP Schiff bases in the concentration of 1.0×10^{-4} M, were also listed in Table 5.

According to Fukui's frontier molecular orbital theory [38], reactive ability of the inhibitor is related with frontier molecular orbital (MO), including highest occupied molecular orbital (HOMO) and lowest unoccupied molecular orbital (LUMO). Higher HOMO energy (E_{HOMO}) of the adsorbent leads to higher electron donating ability [39–41]. Low LUMO energy (E_{LUMO}) indicates that the acceptor accepts electrons easily. Among these Schiff bases, 3-HBP and 4-HBP have the highest HOMO energy, they donate electrons easily, and they have the best inhibitive property but the changing tendency of 3-HBP and 4-HBP is not correlated to inhibition efficiencies. So in these systems, the theoretical parameters E_{HOMO} cannot be used to predicate the inhibition efficiencies of the inhibitors. On the other hand, E_{LUMO} values of three Schiff bases increased in the order: 2-HBP < 4-HBP < 3-HBP. These results agree with the experimental observations, which imply that 3-HBP compound has better corrosion performance (Fig. 10A).

The energy gap between LUMO and HOMO ($\Delta E = E_{\text{LUMO}} - E_{\text{HOMO}}$) is an important stability index [42]. The smaller is the value of ΔE , the more probable it is that the molecule has inhibition efficiencies. The results obtained from quantum chemical calculation using B3LYP/6-31G(d,p) are listed in Table 5 that are in a good agreement with experimental results (Fig. 10B).

From the quantum chemical point, the fraction of electronic charge (ΔN) transferred from the inhibitor to the metal is another important factor [43]. When a bulk metal and an organic corrosion inhibitor are brought together, electron flow will occur from the atom of the lower χ value to the atom of the higher χ value until the chemical potentials become equal. Then, ΔN , the fraction of charge transferred, may be written as:

$$\Delta N = \frac{\chi_M - \chi_I}{2(\eta_M + \eta_I)} \quad (5)$$

where the subscripts *M* and *I* represent the metal and inhibitor, respectively. According to Pearson, operational and approximate definitions of the electronic chemical potential (μ) and the absolute hardness (η) of a chemical system are given by [44]:

$$-\mu = \frac{(I + A)}{2} = \chi \quad (6)$$

$$\eta = \frac{(I - A)}{2} \quad (7)$$

where *I* is the ionization potential and *A* is the electron affinity. Since $(I + A)/2$ is the Mulliken electronegativity for atoms, the value of χ for any system is known as the absolute electronegativity. According to Koopman's theorem, the frontier orbital energies are given by [45]:

$$I = -E_{\text{HOMO}} \quad (8)$$

$$A = -E_{\text{LUMO}} \quad (9)$$

The percent inhibition of steel with *n*-HBP Schiff bases inhibitors shows good correlation with the electronic chemical potential,

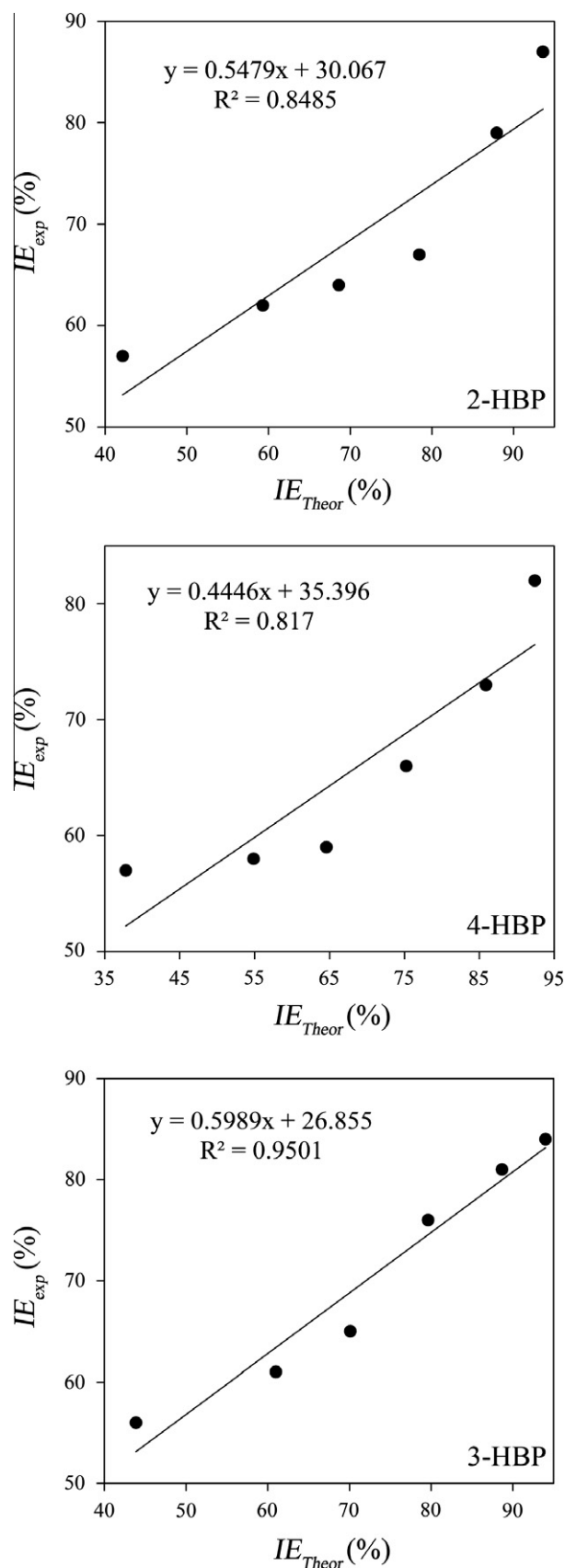


Fig. 12. Correlation of experimental and theoretical inhibition efficiencies of the studied Schiff bases using the B3LYP/6-31G(d,p) method.

as depicted in Fig. 10C. It is interesting to note that the percent inhibition increases progressively with an increase the electronic chemical potential ($R^2 = 0.66$).

Using a theoretical χ_M value of 7 eV mol^{-1} and η_M value of 0 eV mol^{-1} for iron atom [43], ΔN , the fraction of electrons transferred from inhibitor to the iron molecule, was calculated and listed in Table 5. The values of ΔN clearly revealed that the inhibition efficiency increased with the ΔN increase (Fig. 10D). According to other reports [43,46], values of ΔN showed inhibition effect resulted from electrons donation.

Agreeing with Lukovits's study [46], if $\Delta N < 3.6$, the inhibition efficiency increases with increasing electron-donating ability at the metal surface. In this study, the three Schiff bases are the donators of electrons, and the iron surface is the acceptor. The compounds are bound to the metal surface, and thus form an inhibition adsorption layer against corrosion. The molecule 3-HBP has the highest inhibition efficiency because it has the lowest LUMO energy, the electronic chemical potential, ΔE and ΔN values, and it has the greatest ability of offering electrons, and 2-HBP has the lowest inhibition efficiency, for vice versa.

The Mulliken charge populations and the direction of dipole moment calculated for the three Schiff bases are projected to the molecular plane. The charge population and direction of the dipole moment can be understood by considering the electrostatic potential (middle and right panels of Fig. 11), which discerns electron density rich regions centered on O atoms in hydroxyl group, N atoms in —C=N— group and C atoms of carbon bone chain and some of carbon atoms of benzene rings. The regions of highest electron density are generally the sites to which electrophiles attacked. So O, N, and C atoms are the active center, respectively, which have the strongest ability of bonding to the metal surface. On the other side, HOMO (Fig. 9) was mainly distributed over the mentioned atoms. Thus, these areas are probably the primary sites of the bonding.

3.5. Quantitative structure activity relation (QSAR) study

From the present study, it has been established that the mechanism of inhibition involves the donation of electron to Fe in mild steel by the electron. However, it has also been found that the inhibitor can not only donate electron to the metal but can also accept electron from the lone pair of Fe, leading to the formation of a feedback bond [47]. The formation of a feedback bond can be analyzed by considering a quantitative relationship between the E_{HOMO} , E_{LUMO} and the experimental inhibition efficiency. The considerations led to the establishment of Eqs. (10)–(13) for B3LYP/6-31G(d,p), B3LYP/3-21G, HF/6-31G(d,p) and HF/3-21G, respectively.

$$IE_{\text{exp}} = 2.48E_{\text{HOMO}} - 0.57E_{\text{LUMO}} + 14.88 \quad (10)$$

$$IE_{\text{exp}} = 2.66E_{\text{HOMO}} - 0.23E_{\text{LUMO}} + 16.03 \quad (11)$$

$$IE_{\text{exp}} = 0.66E_{\text{HOMO}} - 1.73E_{\text{LUMO}} + 11.16 \quad (12)$$

$$IE_{\text{exp}} = 0.77E_{\text{HOMO}} - 2.7E_{\text{LUMO}} + 15.37 \quad (13)$$

From the above equations, it can be seen that the coefficients of the E_{HOMO} are positive while that of E_{LUMO} are negative indicating that the formation of a feedback bond is favored by increasing value of E_{HOMO} but with decreasing value of E_{LUMO} . Correlations between the above equations and experimental inhibition efficiencies are excellent ($R^2 = 1$). However, when all the calculated quantum chemical parameters are used for developing suitable models for the different computational methods (through the multiple regression), it is not possible to obtain simple equations such as those given in Eqs. (10)–(13). This indicates that corrosion inhibition process is a composite function of some quantum chemical descriptors.

Though a number of satisfactory correlations have been reported by other investigators [43,48–51] between the inhibition efficiency of various inhibitors used and some quantum chemical parameters, a composite index and a combination of more than one parameter [52,53] has been used to perform QSAR which might affect the inhibition efficiency of the studied molecules. Consequently, a relation may exist between the composite index and the average corrosion inhibition efficiency for a particular inhibitor molecule. Therefore, for this study, parameters have been selected relevant to the activity of the molecules under investigation. The linear model approximates inhibition efficiency ($IE_{\text{Theor}}\%$) as in the equation below:

$$IE_{\text{Theor}} = Ax_i C_i + B \quad (14)$$

where IE_{Theor} is the inhibition efficiency, A and B are the regression coefficients determined by regression analysis, x_i is a characteristic quantum index for the inhibitor molecule (i), and C_i denotes the experiment's concentration of the inhibitor. Such linear approach was not found to be satisfactory for correlating the present results. Consequently, the nonlinear model (NLM) proposed by Lukovits et al. [54] and also used by Khaled [53] for studying the interaction of corrosion inhibitors with metal surfaces in acidic solutions derived from the equation below (15) based on the Langmuir adsorption isotherm has been used:

$$IE_{\text{Theor}} = \frac{(Ax_i + B)C_i}{1 + (Ax_i + B)C_i} \times 100 \quad (15)$$

where IE_{Theor} is the inhibition efficiency, A and B are the regression coefficients determined by regression analysis, x_i is a quantum chemical index characteristic for the molecule (i) and C_i denotes the experimental concentration i . Application of equation 15 for 3-HBP Schiff base yields Eqs. (16)–(19) for B3LYP/6-31G(d,p), B3LYP/3-21G, HF/6-31G(d,p) and HF/3-21G methods, respectively.

$$IE_{\text{Theor}} = \frac{(-9.11E_{\text{HOMO}} - 1.17E_{\text{LUMO}} + 8.93\Delta E + 2.23\Delta N + 10.19\mu + 364.47V + 1)C_i}{1 + (-9.11E_{\text{HOMO}} - 1.17E_{\text{LUMO}} + 8.93\Delta E + 2.23\Delta N + 10.19\mu + 364.47V + 1)C_i} \times 100 \quad (16)$$

$$IE_{\text{Theor}} = \frac{(-9.57E_{\text{HOMO}} - 1.26E_{\text{LUMO}} + 9.31\Delta E + 2.29\Delta N + 10.58\mu + 380.88V + 1.08)C_i}{1 + (-9.57E_{\text{HOMO}} - 1.26E_{\text{LUMO}} + 9.31\Delta E + 2.29\Delta N + 10.58\mu + 380.88V + 1.08)C_i} \times 100 \quad (17)$$

$$IE_{\text{Theor}} = \frac{(-11.06E_{\text{HOMO}} - 0.55E_{\text{LUMO}} + 11.51\Delta E + 2.32\Delta N + 11.47\mu + 408.13V + 1.23)C_i}{1 + (-11.06E_{\text{HOMO}} - 0.55E_{\text{LUMO}} + 11.51\Delta E + 2.32\Delta N + 11.47\mu + 408.13V + 1.23)C_i} \times 100 \quad (18)$$

$$IE_{\text{Theor}} = \frac{(-11.22E_{\text{HOMO}} - 0.43E_{\text{LUMO}} + 11.79\Delta E + 2.32\Delta N + 11.48\mu + 411.57V + 1.25)C_i}{1 + (-11.22E_{\text{HOMO}} - 0.43E_{\text{LUMO}} + 11.79\Delta E + 2.32\Delta N + 11.48\mu + 411.57V + 1.25)C_i} \times 100 \quad (19)$$

The same results are obtained for other Schiff bases. From the results obtained, it can be seen that there is a good and acceptable coefficient correlation between the experimental and calculated/estimated inhibition efficiencies of the studied Schiff bases using the B3LYP/6-31G(d,p) method as shown in Fig. 12. Also it is neces-

sary to mention that there is no general way of predicting compounds usefulness to be a good corrosion inhibitor or find some universal type of correlation. A number of excluded parameters that should be involved such as effect of solvent molecules, surface nature, adsorption sites of the metal atoms or oxides sites or

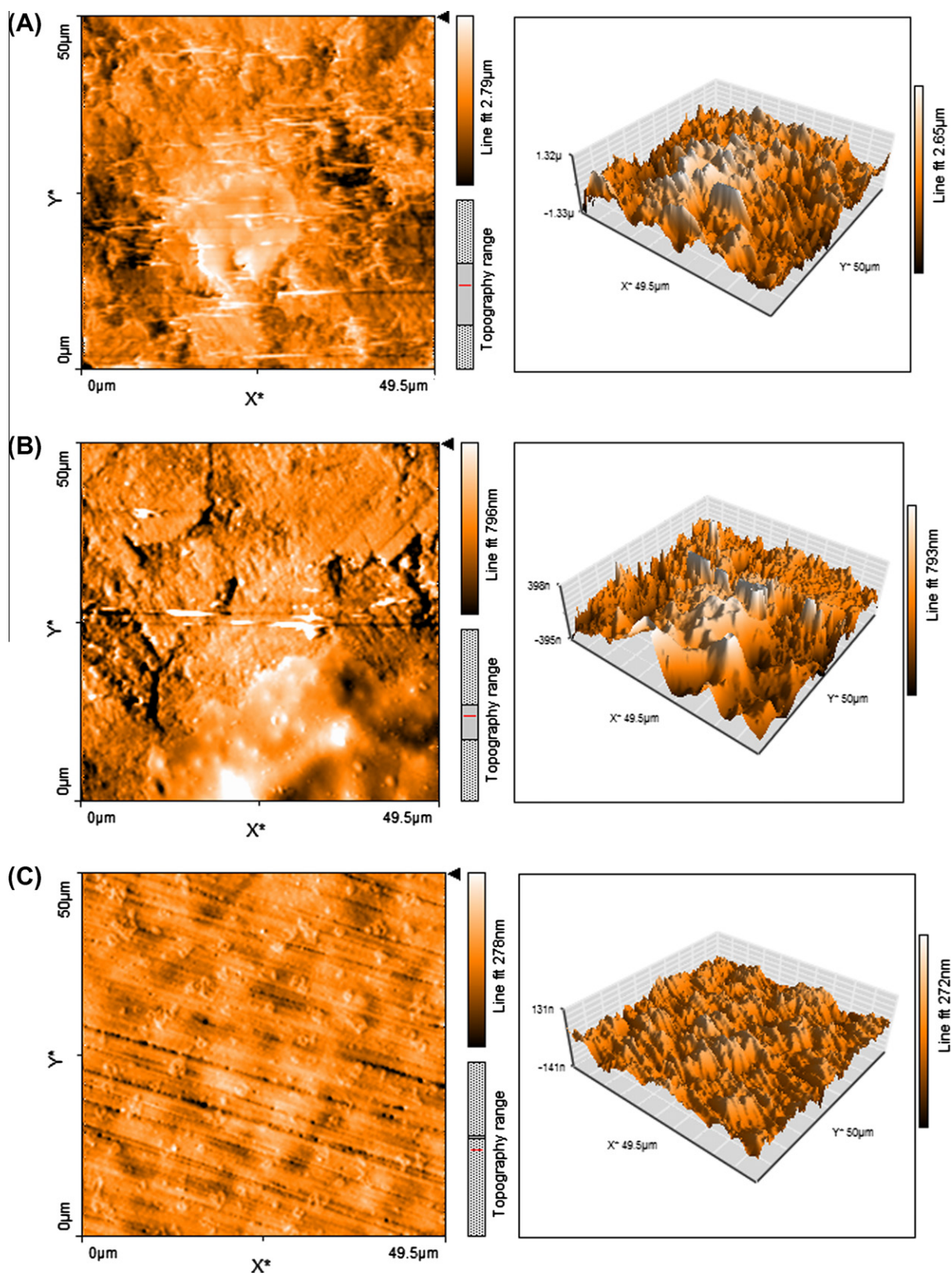


Fig. 13. 2D and 3D of AFM images of steel exposed to 1 M HCl solution (a), in the presence of 2×10^{-4} M of 2-HBP (b), 3-HBP (c), 4-HBP (d) (scan size: $49.5 \times 50 \mu$).

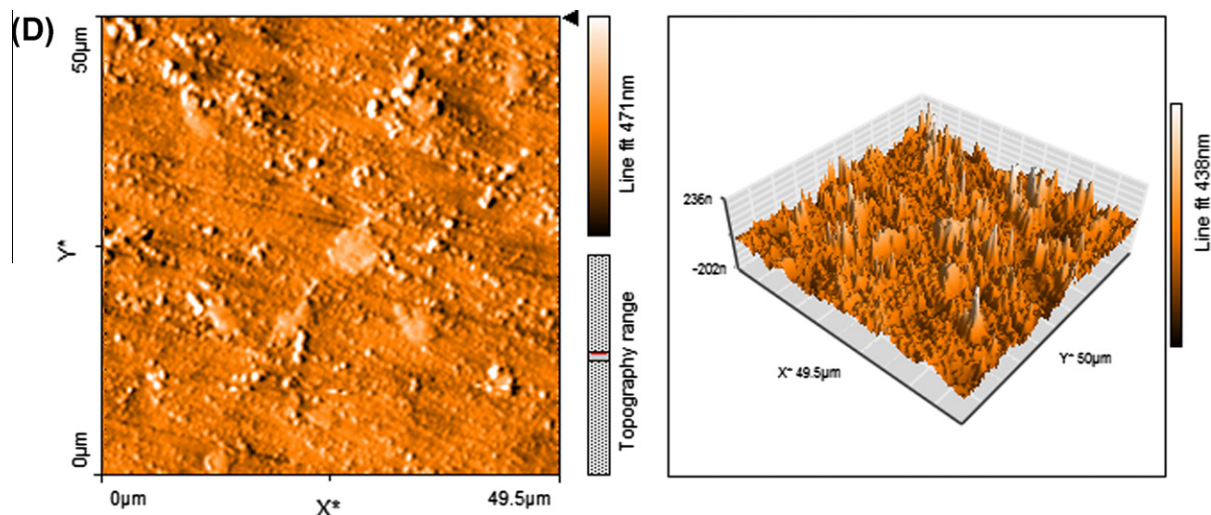


Fig. 13. (continued)

vacancies, competitive adsorption with other chemical species in the fluid phase and solubility must also be given due consideration. However, the quintessential component of the QSAR approach is the determination of the correct molecular descriptors.

3.6. Surface analysis

The two (2D) and three-dimensional (3D) AFM images of steel surface after exposure to 1 M HCl solution for 1 day is given in Fig. 13a. As it is shown in Fig. 13a, the surface of steel electrode exposed to corrosive solution has a considerably porous structure with large and deep pores. The roughness of surface is 2.65 μm . However, the surface is smoother in the presence of 2×10^{-3} M 2-HBP, 2×10^{-4} M 3-HBP and 4-HBP separately (Fig. 13b–d), which suggests adsorption of inhibitor molecules on the steel surface and reduces the corrosion rate [55]. The surface roughness of steel after the addition of 2-HBP, 3-HBP and 4-HBP are 793, 272 and 438 nm, respectively.

4. Conclusion

Effect of hydroxyl group position on adsorption behavior and corrosion inhibition of 2-, 3- and 4-Hydroxybenzaldehyde Schiff base has been studied on steel electrode in 1 M HCl by using electrochemical technique and quantum calculations. Comparative study of these inhibitors show that the inhibition efficiency follows the order: 3-HBP > 4-HBP > 2-HBP and the order of protection effect is the same for both electrochemical and computational methods. Impedance measurements indicate that with increasing inhibitors concentration, the polarization resistance (R_{ct}) increased, while the double layer capacitance (C_{dl}) decreased.

Through the quantum chemical calculations, it was shown that calculated parameters were correlated with the experimental results, and it was found that inhibition efficiency increased with the lower E_{LUMO} and $\Delta E_{LUMO} - E_{HOMO}$ values. The variation in the protection ability of three Schiff bases can be attributed to their spatial molecular structure and molecular electronic structure. Furthermore, electronegative oxygen and nitrogen atoms facilitate the adsorption of the molecule on the steel surface.

The AFM micrographs show the smoother surface for inhibited metal samples rather than uninhibited samples due to the formation of film on the inhibited surface and best inhibition was obtained in presence of 3-HBP.

By studying the effects of hydroxyl groups in ortho-, meta-, para- positions, the best one as inhibitor was found to be meta-position of OH in Schiff base (i.e., 3-HBP).

References

- [1] I. Ahamad, R. Prasad, M.A. Quraishi, Corros. Sci. 52 (2010) 933.
- [2] S. Issaadi, T. Douadi, A. Zouaoui, S. Chafaa, M.A. Khan, G. Bouet, Corros. Sci. 53 (2011) 1484.
- [3] R. Solmaz, Corros. Sci. 52 (2010) 3321.
- [4] I. Ahamad, Mater. Chem. Phys. 124 (2010) 1155.
- [5] P. Lowmunkhong, D. Ungtharak, P. Sutthivaiyakit, Corros. Sci. 52 (2010) 30.
- [6] K.C. Emregu, E. Duzgun, O. Atakol, Corros. Sci. 48 (2006) 3243.
- [7] S.M.A. Hosseini, A. Azimi, Mater. Corros. 59 (1) (2008) 41.
- [8] R. Solmaz, E. Altunbas, G. Kardas, Mater. Chem. Phys. 125 (2011) 796.
- [9] A.M. Badiea, K.N. Mohana, Corros. Sci. 51 (2009) 2231.
- [10] K. Stanly Jacob, G. Parameswaran, Corros. Sci. 52 (2010) 224.
- [11] R. Hasanov, Appl. Surf. Sci. 253 (2007) 3913.
- [12] R.A. Prabhu, T.V. Venkatesha, A.V. Shanbhag, G.M. Kulkarni, R.G. Kalkhambkar, Corros. Sci. 50 (2008) 3356.
- [13] A. Stoyanova, G. Petkova, S.D. Peyerimhoff, Chem. Phys. 279 (2002) 1.
- [14] A.Y. Musa, A.A.H. Kadhum, A.B. Mohamad, A.A.B. Rahoma, H. Mesmari, J. Mol. Struct. 969 (2010) 233.
- [15] L.T. Sein Jr., A.L. Cederberg-Crossley, J. Mol. Struct. 1004 (2011) 319.
- [16] N.O. Obi-Egbedi, I.B. Obot, M.I. El-Khaiary, J. Mol. Struct. 1002 (2011) 86.
- [17] S.A. Fairhurst, D.L. Hughes, U. Kleinkes, G.J. Leigh, J.R. Sanders, J. Weisner, J. Chem. Soc. Dalton Trans. (1995) 321.
- [18] Gaussian 03, Revision B.03, M.J. Frisch, G.W. Trucks, H.B. Schlegel, G.E. Scuseria, M.A. Robb, J.R. Cheeseman, J.A. Montgomery, Jr., T. Vreven, K.N. Kudin, J.C. Burant, J.M. Millam, S.S. Iyengar, J. Tomasi, V. Barone, B. Mennucci, M. Cossi, G. Scalmani, N. Rega, G.A. Petersson, H. Nakatsuji, M. Hada, M. Ehara, K. Toyota, R. Fukuda, J. Hasegawa, M. Ishida, T. Nakajima, Y. Honda, O. Kitao, H. Nakai, M. Klene, X. Li, J.E. Knox, H.P. Hratchian, J.B. Cross, C. Adamo, J. Jaramillo, R. Gomperts, R.E. Stratmann, O. Yazyev, A.J. Austin, R. Cammi, C. Pomelli, J.W. Ochterski, P.Y. Ayala, K. Morokuma, G.A. Voth, P. Salvador, J.J. Dannenberg, V.G. Zakrzewski, S. Dapprich, A.D. Daniels, M.C. Strain, O. Farkas, D.K. Malick, A.D. Rabuck, K. Raghavachari, J.B. Foresman, J.V. Ortiz, Q. Cui, A.G. Baboul, S. Clifford, J. Cioslowski, B.B. Stefanov, G. Liu, A. Liashenko, P. Piskorz, I. Komaromi, R.L. Martin, D.J. Fox, T. Keith, M.A. Al-Laham, C.Y. Peng, A. Nanayakkara, M. Challacombe, P.M.W. Gill, B. Johnson, W. Chen, M.W. Wong, C. Gonzalez, J.A. Pople, Gaussian, Inc., Pittsburgh PA, 2003.
- [19] P. Geerlings, F.D. Proft, W. Langenaeker, Chem. Rev. 103 (2003) 1793.
- [20] C. Lee, W. Yang, R.G. Parr, Phys. Rev. B 37 (1988) 785.
- [21] G.A. Petersson, M.A. Al-Laham, J. Chem. Phys. 94 (1991) 6081.
- [22] G.A. Petersson, A. Bennett, T.G. Tensfeldt, M.A. Al-Laham, W.A. Shirley, J. Mantzaris, J. Chem. Phys. 89 (1988) 2193.
- [23] J.R. MacDonald, Solid State Ionics 13 (1984) 147.
- [24] I. Danaee, M. Jafarian, F. Forouzandeh, F. Gopal, M.G. Mahjani, J. Phys. Chem. B 112 (2008) 15933.
- [25] N.A. Negm, Y.M. Elkholi, M.K. Zahran, S.M. Tawfik, Corros. Sci. 52 (2010) 3523.
- [26] N.A. Negm, F.M. Ghuiba, S.M. Tawfik, Corros. Sci. 53 (2011) 3566.
- [27] M.A. Hegazy, Corros. Sci. 51 (2009) 2610.
- [28] K. Mallaiya, R. Subramaniam, S.S. Srikandan, Electrochim. Acta 56 (2011) 3857.
- [29] M.A. Migahed, I.F. Nassar, Electrochim. Acta. 53 (2008) 2877.
- [30] H. Keles, Mater. Chem. Phys. 130 (2011) 1317.
- [31] K.C. Emregül, O. Atakol, Mater. Chem. Phys. 82 (2003) 188.

- [32] I. Danaee, J. Electroanal. Chem. 662 (2011) 415.
- [33] I. Danaee, S. Noori, Int. J. Hydrogen Energy 36 (2011) 12102.
- [34] I.B. Obot, N.O. Obi-Egbedi, S.A. Umoren, Corros. Sci. 51 (2009) 276.
- [35] I.B. Obot, N.O. Obi-Egbedi, Colloids Surf. A 330 (2008) 207.
- [36] G. Gece, Corros. Sci. 50 (2008) 2981.
- [37] M. Ozcan, F. Karadağ, İ. Dehri, Colloids Surf. A 316 (2008) 55.
- [38] H. Fujimoto, Sh. Kato, Sh. Yamabe, K. Fukui, Chem. Phys. 60 (1974) 572.
- [39] N. Khalil, Electrochim. Acta 48 (2003) 2635.
- [40] J. Vosta, N. Hackerman, Corros. Sci. 30 (1990) 949.
- [41] I. Lukovits, K. Pálfi, I. Bakó, E. Kálmán, Corrosion 53 (1997) 915.
- [42] D.F.V. Lewis, C. Ioannides, D.V. Parke, Xenobiotica 24 (1994) 401.
- [43] V.S. Sastri, J.R. Perumareddi, Corrosion 53 (1997) 617.
- [44] R.G. Pearson, Inorg. Chem. 27 (1988) 734.
- [45] M.J.S. Dewar, W. Thiel, J. Am. Chem. Soc. 99 (1977) 4899.
- [46] I. Lukovits, E. Kálmán, Corrosion 57 (2001) 3.
- [47] N.O. Eddy, U.J. Ibok, E.E. Ebenso, J. Appl. Electrochem. 40 (2010) 445.
- [48] J.M. Costa, J.M. Llush, Corros. Sci. 24 (1984) 924.
- [49] D. Wang, S. Li, Y. Ying, M. Wang, H. Xiao, Z. Chen, Corros. Sci. 41 (1999) 1911.
- [50] S.L. Li, Y.G. Wang, S.H. Chen, R. Yu, S.B. Lei, H.Y. Ma, D.X. Liu, Corros. Sci. 41 (1999) 1769.
- [51] J. Cruz, E. Garcia-Ochoa, M. Castro, J. Electrochem. Soc. 150 (2003) B26.
- [52] K.F. Khaled, K. Babic-Samradzija, N. Hackerman, Electrochim. Acta 50 (2005) 2515.
- [53] K.F. Khaled, Appl. Surf. Sci. 252 (2006) 4120.
- [54] I. Lukovits, E. Kalman, F. Zucchi, Corrosion (NACE) 57 (2001) 3.
- [55] H. Keles, M. Keleş, I. Dehri, O. Serindag, Mater. Chem. Phys. 112 (2008) 173.